Soft Matter

PAPER

View Article Online
View Journal | View Issue

Cite this: *Soft Matter*, 2016, 12, 7539

Mesoporous self-assembled nanoparticles of biotransesterified cyclodextrins and nonlamellar lipids as carriers of water-insoluble substances†

Leïla Zerkoune,[a] Sylviane Lesieur,[a] Jean-Luc Putaux,[bc] Luc Choisnard,[de] Annabelle Gèze,[de] Denis Wouessidjewe,[de] Borislav Angelov,[f] Corinne Vebert-Nardin,[g] James Doutch[h] and Angelina Angelova*[a]

Received 17th March 2016,
Accepted 19th August 2016

DOI: 10.1039/c6sm00661b

www.rsc.org/softmatter

Soft mesoporous hierarchically structured particles were created by the self-assembly of an amphiphilic deep cavitand cyclodextrin βCD-*n*C_{10} (degree of substitution *n* = 7.3), with a nanocavity grafted by multiple alkyl (C_{10}) chains on the secondary face of the βCD macrocycle through enzymatic biotransesterification, and the nonlamellar lipid monoolein (MO). The effect of the non-ionic dispersing agent polysorbate 80 (P80) on the liquid crystalline organization of the nanocarriers and their stability was studied in the context of vesicle-to-cubosome transition. The coexistence of small vesicular and nanosponge membrane objects with bigger nanoparticles with inner multicompartment cubic lattice structures was established as a typical feature of the employed dispersion process. The cryogenic transmission electron microscopy (cryo-TEM) images and small-angle X-ray scattering (SAXS) structural analyses revealed the dependence of the internal organization of the self-assembled nanoparticles on the presence of embedded βCD-*n*C_{10} deep cavitands in the lipid bilayers. The obtained results indicated that the incorporated amphiphilic βCD-*n*C_{10} building blocks stabilize the cubic lattice packing in the lipid membrane particles, which displayed structural features beyond the traditional CD nanosponges. UV-Vis spectroscopy was employed to characterize the nanoencapsulation of a model hydrophobic dimethylphenylazo-naphthol guest compound (Oil red) in the created nanocarriers. In perspective, these dual porosity carriers should be suitable for co-encapsulation and sustained delivery of peptide, protein or siRNA biopharmaceuticals together with small molecular weight drug compounds or imaging agents.

Introduction

Biocompatible mesoporous hierarchically ordered nanoassemblies are highly desirable for modern applications involving multi-material building blocks.[1–5] Among them, liquid crystalline structures display considerable advantages for the transport and delivery of diverse kinds of active molecules and pharmaceuticals.[6–11] Soft porous nanocarriers with tunable properties may be easily fabricated by the self-assembly of lipids and amphiphiles of appropriate chemical structures and functionalities.[12–15] The nanoporous organization of the carriers may be particularly efficient for encapsulation and protection of fragile hydrophobic guest molecules of various dimensions.[16]

PEGylated and sterically stabilized cubosome, hexosome and spongosome liquid crystalline carriers formed upon hydration of nonlamellar lipid mixtures have demonstrated high capacity for entrapment of protein, DNA and siRNA therapeutics as well as of small molecular weight compounds.[3–9,11] The aqueous channel networks in the cubosome carriers govern the molecular uptake and diffusion of hydrosoluble guest entities.[4,11–13] Depending on the amphiphilic composition, cubic lattice parameters of the mesostructures have determined nanochannel diameters in the range between 2 and 7 nm.[4,11–13] The release of encapsulated molecules may occur in a controlled

[a] *Institut Galien Paris-Sud, CNRS UMR 8612, Univ. Paris-Sud, Université Paris-Saclay, LabEx LERMIT, 5 rue J.-B. Clément, 92296 Châtenay-Malabry cedex, France. E-mail: Angelina.Angelova@u-psud.fr*
[b] *Université Grenoble Alpes, Centre de Recherches sur les Macromolécules Végétales (CERMAV), F-38000 Grenoble, France*
[c] *CNRS, CERMAV, F-38000 Grenoble, France*
[d] *Université Grenoble Alpes, Département de Pharmacologie Moléculaire (DPM), F-38000 Grenoble, France*
[e] *CNRS UMR 5063, DPM, F-38000 Grenoble, France*
[f] *Institute of Physics, ELI Beamlines, Academy of Sciences of the Czech Republic, Na Slovance 2, CZ-18221 Prague, Czech Republic*
[g] *IPREM/EPCP, Technopole Helioparc, 2 Av. Pdt Angot, 64053 PAU cedex 09, France*
[h] *Diamond Light Source Ltd., Didcot, Oxfordshire, OX11 0DE, UK*

† Electronic supplementary information (ESI) available: Physico-chemical characteristics (Table S1), the chemical structure of Oil red O (OR) (Fig. S1) and additional results from quasi-elastic light scattering, POM, UV-Visible spectroscopy and optical density measurements (Fig. S2–S11). See DOI: 10.1039/c6sm00661b

manner as a function of the internal structural organization of the nanocarriers.[1,3,10,15] Lipid-membrane based nanochannelled carriers (*e.g.* cubosomes and spongosomes) have been used for the solubilization of hydrophobic guest compounds as well. Entrapment efficiencies of up to 95% have been reported for bioactives of rather low aqueous solubilities.[1,5–8,16b]

Besides nanochanneled lipid-based carriers, nanoporous materials shaped as nanosponges have been fabricated from β-cyclodextrins (βCDs).[17] Cyclodextrin nanosponges and cyclodextrin-based hybrid assemblies have shown interesting properties for multi-drug delivery, which may combine bioactives exerting additive therapeutic effects.[18–24] In these studies, the affinity of the drugs for the CD nanocavity has been of crucial importance for the inclusion complexation in a nanostructured environment.[18,19] In addition, the encapsulation capacity of the carriers for hydrophobic drugs might be limited by the size of the βCD nanocavity, which is around 0.8 nm (ESI,† Table S1).

Engineering of the primary and/or the secondary faces of native CD macrocycles has been performed through enzymatic biotransesterification or by chemical modifications towards fabrication of novel kinds of amphiphilic CD nanostructures.[25–32] It has been shown that CD deep cavitands of amphiphilic nature may self-assemble into nanoparticles alone or in combinations with other amphiphiles.[18,25–30] Deep cavitand building blocks easily formed mixed nanoassemblies with lipids.[16a,29] Nanostructured supramolecular CD scaffolds have been studied in diverse nanomedical applications aiming at targeting of the blood brain barrier (BBB), healing of neurodiseases, gene transfection, gene silencing, phototherapy, and transport of anti-cancer drugs.[18–24,32]

Recently, self-assembled nanocarriers of dual porosity type have been designed through encapsulation of membrane barrel proteins, such as the porin OmpF, in an inverted hexagonal liquid crystalline lipid phase.[2a] The latter involves hexagonally-packed aqueous tubes surrounded by lipid monolayers. The water-filled pores, engineered *via* the OmpF barrels in the lipid phase, are characterized by a diameter of around 1.1 nm. Low OmpF amounts of 0.24 and 0.5 wt% have been sufficient to induce the formation of perforated mesophases in the monolinolein–tetradecane–OmpF system and to modify its transport properties.[2a]

An alternative possibility to augment the nanoporosity of the lipid carriers is to employ deep cavitand vase-like molecules[16a] and nanoarchitectonics and interfacial engineering principles.[33,34] Embedded deep cavitands may control the entrapment of large hydrophobic molecules in the generated multicompartment host lipid assemblies. Thus, the inclusion of deep-cavitand building blocks (Fig. 1) in amphiphilic nanocarriers may enhance the stability of encapsulated fragile hydrophobic molecules, and in some cases, their photophysical properties.[29a] It may be suggested that supramolecular lipid/cyclodextrin assemblies will be excellent systems for solubilization and protection of unstable drugs. As a matter of fact, controlled drug delivery systems, used for co-delivery or for multi-drug delivery, can strongly improve the therapeutic outcomes through synergistic effects.[35–38]

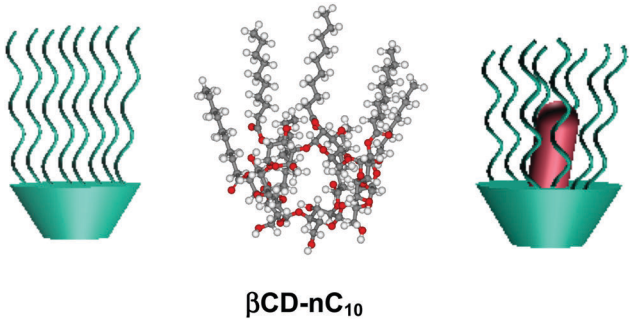

Fig. 1 Schematic presentation of a vase-like deep cavitand amphiphile (left) and the actual chemical structure of the amphiphilic biotransesterified cyclodextrin derivative βCD-nC_{10} (MW 2266; the degree of substitution of the cyclodextrin ring by decanoate chains n = 7.3) studied in this work (middle). (Right): Inclusion of a fragile hydrophobic guest molecule in the deep cavitand space. The cyclodextrin cage may impart porosity to host lipid membranes.

The present work employs CD-driven amphiphile nanoarchitectonics to design nanocarriers of soft nature through the self-assembly of the nonlamellar monoglyceride lipid monoolein (MO) and the vase-like deep cavitand derivative βCD-nC_{10} (Fig. 1). Deep-cavitand amphiphilic CD building blocks βCD-nC_{10} (n = 7.3), produced by enzymatic biotransesterification,[25b] are incorporated into self-assembled membrane-type particles of MO. The lyotropic lipid MO displays rich liquid crystalline phase behaviour upon swelling in the aqueous phase.[39] Its dispersed state involves multicompartment nanoparticles (stabilized by surfactants), in which guest compounds may be entrapped in the lipid bilayers or in the aqueous channels. The incorporation of a polysubstituted vase-like cyclodextrin βCD-nC_{10} (with a hydrophobic deep cavitand space serving as an entry compartment in front of the cyclodextrin nanocavity) (Fig. 1) may be expected to contribute to additional compartmentalization of these self-assembled nanocarriers. Polysorbate 80 (P80) was chosen as a dispersion agent and a stabilizer of the generated nanoparticles because it may impart them both stealth and non-haemolytic properties.[25a,40] Dual loaded nanocarriers were prepared through encapsulation of Oil red (a model water-insoluble drug compound with interesting photophysical properties) in βCD-nC_{10}-functionalized lipid membrane nanoassemblies (see the chemical structure of Oil red [1-[2,5-dimethyl-4-(2,5-dimethylphenylazo)phenylazo]-2-naphthol] in ESI† Fig. S1). The obtained blank and nanodrug-loaded multi-material aqueous dispersions were investigated by cryo-transmission electron microscopy (cryo-TEM) imaging, small-angle X-ray scattering (SAXS), quasi-elastic light scattering (QELS), optical density (OD) measurements, and UV-Visible spectroscopy.

Results and discussion

To our knowledge, the organization of nonlamellar lipid membrane particles embedding amphiphilic deep cavitand compounds such as enzymatically-produced polysubstituted

vase-like CDs has not been previously studied. In a first step toward that aim, we prepared self-assembled mixtures of the amphiphilic deep cavitand βCD-nC$_{10}$ (degree of substitution n = 7.3) and the monoglyceride lipid MO, at different molar proportions, in order to establish the compositions corresponding to optically isotropic cubic mesophase assemblies with yet flexible lipid membrane interfaces (see ESI† Fig. S2). Taking into account the hydrophobic nature of the investigated vase-like deep cavitand βCD-nC$_{10}$ (Fig. 1) and its capacity to rigidify the lipid bilayers with a tendency for segregation above a threshold concentration,[29a] we moderately functionalized the bicontinuous cubic membrane of MO by 4 mol% of βCD-nC$_{10}$. This approach aimed at avoiding the phase separation between the amphiphilic CDs and the lipid components.

A cross-polarized optical microscopy (POM) image of the non-dispersed MO/βCD-nC$_{10}$ mixed membrane was obtained (ESI† Fig. S2). The micrograph showed homogeneous and optically isotropic texture of the bulk phase sample studied in the form of a thin liquid crystalline film under cross-polarized light. It reveals that the incorporation of the high molecular weight deep cavitand βCD-nC$_{10}$ amphiphile, with a diameter of the nanocavity of 0.8 nm, is compatible with the cubic nanochannel network of the bicontinuous cubic MO membrane.

For nanoparticle preparation, the quantity of the P80 stabilizer added was varied in the amphiphilic system in the sequence of 5, 10 or 15 mol% P80 at a fixed MO/βCD-nC$_{10}$ content (equal to 4 mol% βCD-nC$_{10}$ deep cavitands with respect to the nonlamellar lipid MO). At this stage, the conditions for optimal dispersion of the bulk liquid crystalline phase into nanoparticles stabilized by a PEGylated corona of P80 were studied with the help of QELS. Selected data from hydrodynamic particle size measurements are shown in ESI† Fig. S3–S8 and also considered in Fig. 6. It is interesting to note that the majority of the dispersions contained two populations of nanoparticles, which corresponded to coexisting vesicles and other types of liquid crystalline assemblies. Vesicular membranes are required for the formation of cubic membrane particles (cubosomes).[4d,8c] Our results indicated that the inclusion of CD macromolecules favors the fraction of the cubosome nanoparticles in the obtained dispersions.

The cryo-TEM images (Fig. 2–4) presented direct evidence for the liquid crystalline topologies of the nanocarriers produced at varying content of the PEGylated surfactant (P80). They distinguished the nanocarriers of inner cubic lattice organization and three-dimensional nanochannel topology. Starting from the highest surfactant content of 15 mol% P80 in the self-assembled mixtures, we established that the 3D bicontinuous cubic MO membrane is destabilized by the included P80 due to a change in the curvature of the lipid/water interfaces. At this relatively high surfactant content, one expects fragmentation of the cubic nanostructure (under physical agitation) into bilayer membrane building blocks, some of which may close into spherical vesicles or nanoscale objects of other topologies (Fig. 2). Generally, the incorporation of large amounts of detergent in the 3D cubic membrane causes its transformation into vesicular assemblies and intermediate nanosponge-type assemblies.

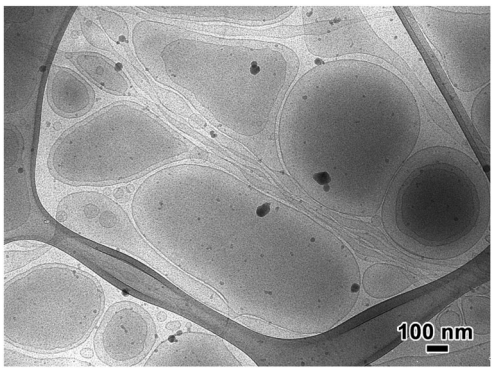

Fig. 2 Cryo-TEM image of self-assembled MO/P80/βCD-nC$_{10}$ nanocarriers containing a 4 mol% βCD-nC$_{10}$ deep cavitand obtained upon dispersion of the lyotropic amphiphilic mixture in the presence of a 15 mol% P80 surfactant agent with respect to the nonlamellar lipid MO. The excess aqueous phase is Milli-Q water. The darks dots are contaminant frost particles.

The cryo-TEM image recorded from the MO/15% P80/βCD-C$_{10}$ system shows spherical, ellipsoidal and elongated-shape membranes with single bilayer or double bilayer peripheries (Fig. 2). Their coexistence with a number of tubular membranes demonstrates the variation of the lipid bilayer curvature upon the transformation of the highly curved 3D cubic lipid assembly into lamellar membrane structures of several intermediate shapes. The observed vesicular morphologies and elongated shapes represent the stages of the solubilization of the periodic bicontinuous cubic membrane by detergent P80. The corresponding hydrodynamic nanoparticle diameters, determined by QELS, are given in ESI† Fig. S3 as raw data. They reveal a broad distribution function of nanoparticle hydrodynamic diameters during the cubic-to-lamellar bilayer transition induced by P80 at the studied concentration. Treatment of the data by a multimodal fitting of the particles populations yielded a bimodal distribution as presented in ESI† Fig. S4c.

It is noteworthy that the βCD-nC$_{10}$ deep cavitand stabilizes the formation of bimembrane and onion-type vesicles with peripheries made of two or three lipid bilayers (Fig. 2 and 3C, D). The generation of such precursors of multilamellar membrane structures is favoured by the propensity of the deep cavitand βCD-nC$_{10}$ nanocavities to form dimers and columnar structures across the adjacent lipid layers.[30a] This structural effect may result in additional layering and structuring of the βCD-functionalized vesicular walls, which adopt a nanoporous organization.

At 10 mol% P80 added to the lipid phase, the blank MO/P80 assemblies displayed fluid membrane morphologies (Fig. 3A and B). The cryo-TEM images established that the dispersion of the bicontinuous cubic lipid membrane in Milli-Q water in the presence of 10 mol% P80 results in vesicular and elongated tubular membrane structures. The observed undulations of the tubular aggregates manifest the dynamic character of the dispersed amphiphilic system and the inhomogeneous distribution of the interfacial curvature. Tubular membranes may further break and rearrange into spherical vesicles (Fig. 3A). Two populations of nanoparticles were identified from the

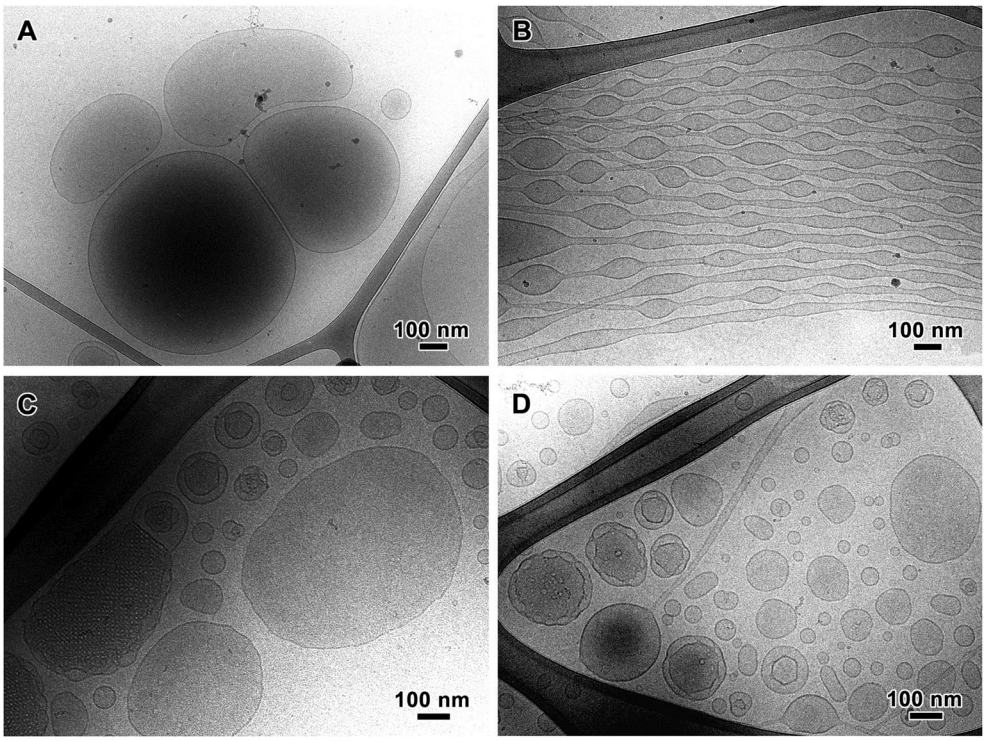

Fig. 3 Cryo-TEM images of self-assembled MO/P80 and MO/P80/βCD-nC_{10} nanocarriers (4 mol% βCD-nC_{10} deep cavitand content) produced through dispersion using a 10 mol% P80 surfactant additive with respect to the nonlamellar lipid MO. (A and B) MO/10 mol% P80 assemblies; (C and D) MO/10 mol% P80/4 mol% βCD-C_{10} assemblies. Aqueous phase: Milli-Q water.

QELS data (ESI† Fig. S4b). They apparently reflect the longitudinal features of the tubular membranes and the approximation of their shapes by equivalent spheres in the fitting algorithm of the QELS software.

A quite dynamic nature of the membrane topologies was also found for the MO/P80/βCD-C_{10} system containing 4 mol% βCD-nC_{10} deep cavitands and 10 mol% P80 (Fig. 3C and D). Vesicular membranes of single bilayer and double membrane topologies were observed to coexist with small and medium-sized cubosome particles. The incorporation of 4 mol% βCD-nC_{10} deep cavitands in the nanostructured MO membrane seems to compensate the effect of the modified interfacial curvature provoked by the added surfactant (10 mol% P80). Notably, βCD-nC_{10} exerts a structuring effect on the lipid bilayers and shifts the phase equilibrium of the membrane assemblies toward packing of lipid bilayers that induces the nucleation and growth of a channel network system within the functionalized particles. The mechanisms of generation and growth of cubosome nanoparticles from membrane building blocks and vesicular membranes have been addressed in detail elsewhere.[3b,8c,10c] The result obtained here evidences that the studied vase-like βCD-nC_{10} amphiphile favours the cubic packing and ordering of the MO bilayers in cubosome-type carriers.

The dispersion and assembly of the monoolein membranes in the presence of 5 mol% P80 yielded a bimodal size distribution by QELS (ESI† Fig. S4a). The latter corresponds to a dynamic coexistence of nanocarriers of two major populations. In accordance with the mechanisms of the vesicle-to-cubosome transition,[3b,4d,8c,10c] the moderate QELS signal at $D_h \sim 80$–150 nm should be associated with the presence of bilayer membranes, whereas the larger QELS signal may be attributed to bigger nanoparticles ($D_h \sim 250$–500 nm) with a dense inner membrane organization (ESI† Fig. S5).

The cryo-TEM images (Fig. 4) confirmed the presence of two main nanocarrier populations in the dispersed system (ESI† Fig. S4 and S5). The images in Fig. 4A and B show that the dispersion of blank nanocarriers MO/P80 (5 mol% P80) comprises small vesicles and nanosponge particles, which coexist with small cubosomal intermediates. The cubosome fraction considerably increases upon the inclusion of 4 mol% βCD-nC_{10} deep cavitands in the lipid phase (Fig. 4C). In the dispersion system MO/5% P80/βCD-C_{10}, the MO/βCD-nC_{10} bicontinuous cubic membranes become highly ordered with no evidence for phase separation of the deep cavitand molecules into detectable clusters within the nanoassemblies.

The fast Fourier transforms (FFTs) of the projected planes of the cubosomes in the cryo-TEM images (Fig. 4C) revealed well-defined cubic packing and two kinds of periodic structures within the cubosome particles. FFT patterns characteristic of primitive cubic and double diamond lattice symmetries were identified. The coexistence of two cubic lattices evidences the mixing events of the deep cavitand amphiphile with the host nonlamellar lipid in the bicontinuous cubic membrane at the studied composition (4 mol% βCD-nC_{10}). In fact, the critical packing parameter of the poly-substituted cyclodextrin with anchored decanoate chains is around 0.9, which defines a

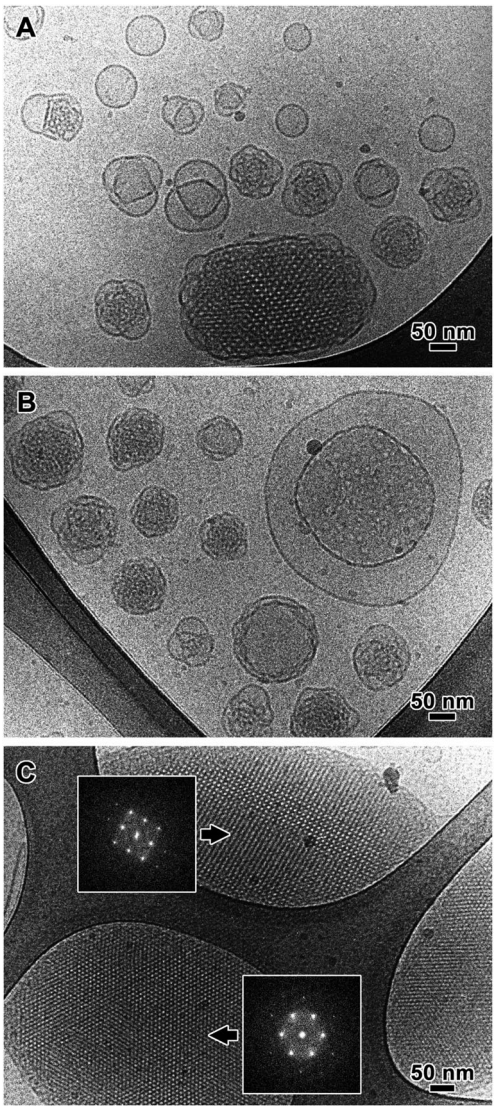

Fig. 4 Cryo-TEM images of self-assembled MO/P80 and MO/P80/β-CD-nC_{10} nanocarriers obtained upon amphiphile dispersion in the presence of a 5 mol% P80 surfactant stabilizer with respect to the nonlamellar lipid MO. (A and B) MO/5 mol% P80 assemblies; (C) MO/5 mol% P80/4 mol% βCD-C_{10} assemblies. Insets: FFT spectra of the regions indicated by arrows. Aqueous phase: Milli-Q water.

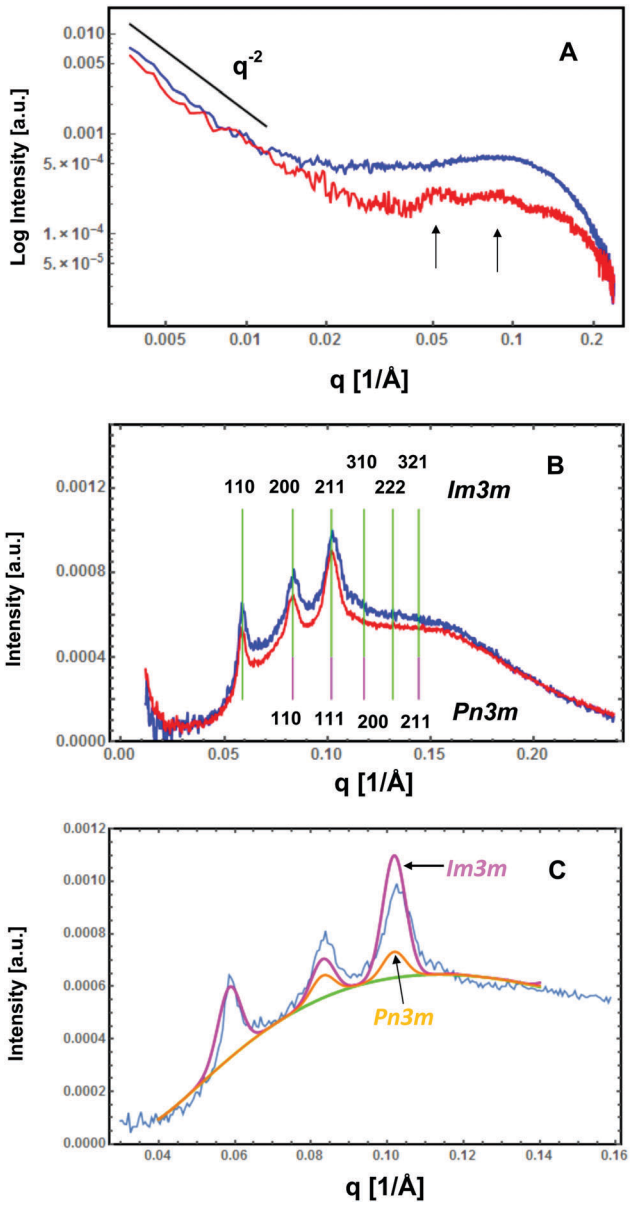

Fig. 5 Synchrotron small-angle X-ray scattering (SAXS) patterns of (A) MO/P80 (5 mol% P80) and (B) MO/P80/βCD-nC_{10} (5 mol% P80; 4 mol% βCD-C_{10} deep cavitand) nanocarriers in the presence (red curves) and absence (blue curves) of loaded hydrophobic guest substance Oil red (OR) at 25 °C. For the purposes of the parallel quantitative spectroscopic determination of nanodrug loading in MO/P80 and MO/P80/βCD-nC_{10} nanocarriers, the content of OR was set at 1 mol% with respect to the nonlamellar lipid MO. The q^{-2} *vs.* q plot is included in (A). The indexing of the positions of the Bragg peaks corresponding to a primitive *Im3m* cubic lattice structure induced in the host double diamond bicontonuous *Pn3m* cubic lattice are denoted by colour bars in (B). These SAXS curves were fitted in (C) by a combination of overlapping Bragg reflections with a dominant contribution from *Im3m* peaks for the studied dispersions of cubosome particles using the Garstecki–Holyst model.[41]

propensity for a lamellar phase formation.[25c] Therefore, homogeneous mixing of βCD-nC_{10} with the nonlamellar lipid MO should decrease the overall curvature of the amphiphilic cubic membrane. The cryo-TEM images reveal that the inclusion of the deep cavitand βCD-nC_{10} in the mixed lipid membrane leads to the formation of a primitive type *Im3m* cubic structure, which is of less negative curvature as compared to that in the initial double diamond type *Pn3m* cubic lattice. The *Pn3m* cubic structure is typical for MO lipid self-assembled in the excess aqueous phase. Therefore, the excess MO phase, which does not accommodate deep cavitand βCD-nC_{10} molecules, may preserve liquid crystalline domains of a double diamond (*Pn3m*) inner cubic membrane packing in the generated self-assembled particles.

Homogeneously dispersed MO/P80 or MO/P80/βCD-nC_{10} nanocarrier systems were analyzed by synchrotron small-angle X-ray scattering (SAXS). Fig. 5A presents the SAXS curves for the MO/P80 nanocarriers containing a 5 mol% P80 surfactant.

The SAXS patterns recorded in the absence of deep cavitands in the nanocarriers display scattering of dispersed membranes rather than Bragg reflections of a periodically ordered cubic lattice. The comparison of the scattering of a smooth surface ($\sim q^{-2}$) with the obtained shape of the scattering curve in Fig. 5A indicated that the studied particles are different from noninteracting membranes. The bilayer membranes appear to fold into precursors of cubosome structures associated with small peaks at q = 0.05–0.09 Å^{-1}. This is consistent with the tendency for the formation of porous interfaces of the nanoparticles (cubosomes), which are stabilized by PEGylated shells of P80. In addition, no oscillation profile typical for monodispersed population of particles was observed. Such patterns have also been obtained for cubosomal intermediates (of diameter D_h below 100 nm), which have been produced through sonication in an ice bath.[3b,6d,8c]

The addition of 4 mol% βCD-nC$_{10}$ deep cavitands to these assemblies transforms their inner organization into a more ordered structure of cubic lattice lipid membrane packing. Fig. 5B shows that the long-range order in the nanoparticles functionalized by amphiphilic cyclodextrin may be characterized by two sets of Bragg peaks. A primitive cubic lattice *Im3m* (Q^{229}) was identified from the sequence of peak positions spaced in the ratio $\sqrt{2}:\sqrt{4}:\sqrt{6}:\sqrt{8}:\sqrt{10}:\sqrt{12}:\sqrt{14}:\sqrt{16}:$ *etc.* and having a first Bragg peak centred at q = 0.058 Å^{-1}. The lattice parameter of the *Im3m* cubic structure was equal to a(*Im3m*) = 15.3 nm. We suggest Bragg peaks indexing with coexisting primitive cubic *Im3m* and double diamond bicontinous cubic *Pn3m* phases. Our SAXS fitting analysis failed to index the obtained patterns by the presence of the primitive only cubic phase in the samples. Fig. 5B demonstrates that there is an overlap of the peaks of the *Im3m* and *Pn3m* cubic phases. The primitive cubic *Im3m* structure appears to be the dominant cubic phase in the obtained mixed assemblies. It displays stronger Bragg peaks in the SAXS patterns (see the peaks fitting in Fig. 5C). A double diamond *Pn3m* (Q^{224}) phase is also present although in a smaller percentage (less intensive reflections) as revealed by the performed peak fitting. In bulk lipid structures, the double diamond bicontinuous cubic phase *Pn3m* shows at least three clear strong peaks with decreasing intensity. They belong to the sequence of Bragg reflections with maxima spaced in the ratio $\sqrt{2}:\sqrt{3}:\sqrt{4}:\sqrt{6}:\sqrt{8}:\sqrt{9}:\sqrt{10}:\sqrt{12}:$ *etc.* In Fig. 5B, this series of Bragg diffraction peaks has an onset at q = 0.088 Å^{-1} and a cubic lattice parameter a(*Pn3m*) = 10.1 nm. Therefore, the data in Fig. 5B reveal that the βCD-nC$_{10}$ deep cavitands induce structural order in the MO/P80 liquid crystalline assemblies and contribute to ordering and packing of the vesicular bilayers into cubic membranes of nonswollen channels (diameter ~4 nm). This effect results from the integration of βCD-nC$_{10}$ into the hydrophobic regions of the lipid membranes. The involved mechanisms are likely related to (i) hydrogen bonding interactions at the lipid/water interfaces and (ii) the capacity of the CD nanocavities to form interlayer dimers, which may favour the lipid membrane fusion into nonlamellar supramolecular structures of nanochannel type.[3b,8c]

It should be noted that in a diluted dispersed system of lipid nanoparticles with an internal periodic structure, the detected Bragg peaks in the SAXS patterns are getting less intense and their number is considerably reduced with regard to that for bulk lipid cubic phases. Dispersions of cubosome particles usually display about three clear Bragg peaks for which the peak assignment may be speculative when the size of the cubosomes is small. The observation of more than three peaks is challenging as the number of cubic lattices inside small cubosome particles is largely insufficient to provide strong reflections in the SAXS patterns. The general features of SAXS patterns of dispersed small cubosome particles, including peak broadening and reduction of the intensity of the smeared peaks as influenced by nanochannel hydration, have been previously discussed in the literature.[5d,8c] Dispersions of cubic nanoparticles with small water channel diameters normally produce SAXS patterns with more clearly defined Bragg peaks and with higher intensities as compared to those for cubosomes with swollen channels.[12b]

Fig. 5C gives further evidence for the presence of coexisting cubic phases in the mixed self-assembled MO/P80/βCD-nC$_{10}$ systems. The obtained value of the mean bilayer thickness was 3.4 nm based on the Garstecki–Holyst fitting model.[41] Thus, both structural methods (cryo-TEM and SAXS) confirmed that the deep cavitand βCD-nC$_{10}$ incorporated into the nonlamellar lipid membrane induces the formation of a primitive cubic lattice *Im3m* structure of a mixed amphiphilic composition. Owing to the fact that the amphiphilic βCD-nC$_{10}$ component is in a deficiency in the nanoassembly, full transformation of the double diamond *Pn3m* type cubic lattice (typical for the MO nanocarriers) into *Im3m* cubic structures of a mixed lipid composition does not occur. The host MO membrane, characterized by *Pn3m* diamond type liquid crystalline structure, seems to saturate by deep cavitand βCD-nC$_{10}$ in the generated nanoparticles.

In subsequent experiments on model drug nanoencapsulation, the amphiphilic MO/P80/βCD-nC$_{10}$ mixtures were loaded with varying quantities of Oil red up to the saturation limit, where phase separation into microscopic clusters occurred. Fig. S2B in the ESI† presents a microscopy image of Oil red-loaded MO/P80/βCD-nC$_{10}$ system (15 mol% OR), in which the excess nonsolubilized hydrophobic guest compound OR is segregated into visibly large areas of microscopic sizes. The performed optical microscopy and optical density (OD) investigations allowed us to determine the concentration range of the components, which would be of interest for the fabrication of homogeneous aqueous dispersions of MO/OR/P80/βCD-nC$_{10}$ nanoassemblies.

We found that the lipophilic OR encapsulated in the apolar compartments of either MO/P80 or MO/P80/βCD-nC$_{10}$ carriers did not influence their overall structural organization. Non-loaded and OR-loaded nanocarriers showed similar structural characteristics in the SAXS patterns (Fig. 5A and B, blue and red plots, respectively). It may be suggested that the lipophilic OR molecules are homogeneously distributed within the lipid membranes of the liquid crystalline nanocarriers.

For the dispersed systems investigated here, quantitative results on nanodrug encapsulation (directly measurable by UV-Visible spectroscopy) were obtained for concentrations of the model compound in the range from 0.5 to 2 mol% OR with respect to the nonlamellar lipid MO. Under these conditions, no dye aggregation was detected. UV-Visible spectra of Oil red at variable dye concentrations were acquired for the MO/P80 and MO/P80/βCD-nC_{10} nanoparticulate systems characterized above by SAXS and cryo-TEM. The same systems were studied by QELS as well. The analysis of the mean hydrodynamic particle sizes of the blank and OR-loaded nanocarrier populations (Fig. 6 and ESI† Fig. S7, S8) demonstrated consistent behaviour with the presented structural data.

The QELS results evidenced bimodal hydrodynamic size distributions in the MO/P80/OR and MO/P80/β-CD-nC_{10}/OR systems corresponding to coexisting populations of small and large nanoparticles of vesicular membrane and cubosomal types, respectively (Fig. 6). Based on the nanoparticles scattering intensities, these data revealed that the inclusion of βCD-nC_{10} deep cavitands in the lipid membranes increases the fraction of the cubosome assemblies, at the expense of small vesicular membranes, independent of the uploaded OR substance.

The encapsulation of OR occurred in the nanocarriers both in the presence and absence of deep cavitands. It may be suggested that the OR loading is supported by all populations in the studied dispersions (cubosomes, vesicles, and nanosponges) as they are built-up by lipid bilayers embedding the guest hydrophobic substance. The OR-loaded βCD-nC_{10}-containing particles (D_h ~ 250–500 nm) appear to be bigger as compared to the OR-loaded vesicles (a population of D_h ~ 80–150 nm detected by QELS). Under these circumstances, it may be expected that the aqueous dispersions containing a greater number of cubosomes of larger sizes might encapsulate more OR guest molecules in the formulation. Generally, the internal cubic membrane, accommodating the hydrophobic model drug, will be better elaborated in large cubosome particles in comparison to the one in single bilayer vesicles. The optical density curves of the blank MO/P80/βCD-nC_{10} and MO/P80 nanocarriers, yet unloaded by OR, demonstrated that the turbidity of the MO/P80/βCD-nC_{10} particle dispersion is higher than that of the initial MO/P80 dispersion (Fig. 7). This also confirms the more densely packed inner organization of the carriers and/or bigger nanoparticle sizes in the case of the βCD-nC_{10} functionalized nanoassemblies.

The nanoencapsulation of Oil red (OR) was studied in self-assembled MO/P80/β-CD-nC_{10} and MO/P80 nanocarriers by

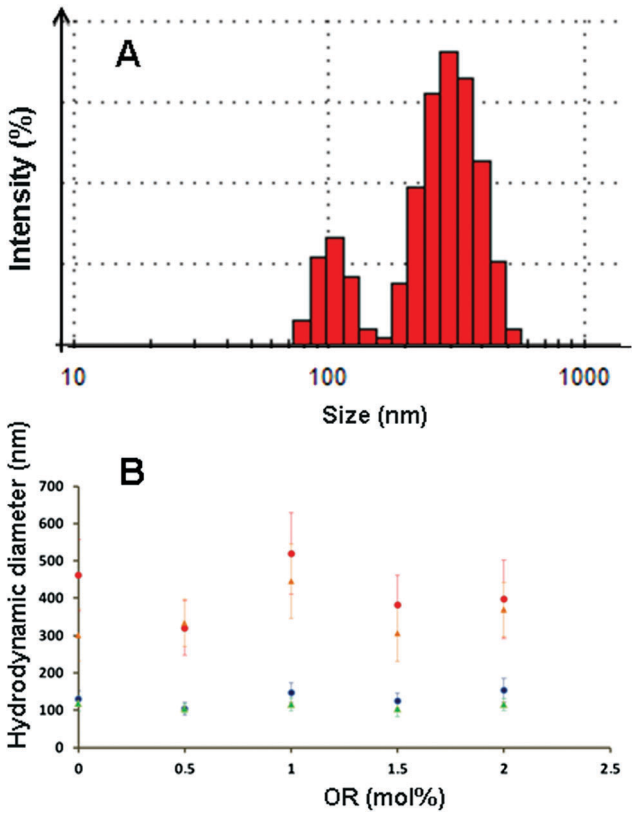

Fig. 6 (A) Quasi-elastic light scattering (QELS) results showing a bimodal distribution of hydrodynamic particle diameters in MO/P80/βCD-nC_{10} dispersed systems loaded with Oil red (OR). (B) Dependence of the hydrodynamic diameters on the molar content of OR. The OR content in the mixed amphiphilic films used for nanocarrier preparation is 0.5, 1, 1.5 and 2 mol% with respect to MO. The triangles indicate the MO/P80/βCD-nC_{10} systems, whereas the circles correspond to MO/P80 systems lacking β-CD-nC_{10}. The two populations of nanoparticles may be attributed to small cubosomal intermediates and vesicular membranes (D_h ~ 80–120 nm) (blue and green symbols), which coexist with well developed liquid crystalline cubic lattice assemblies (cubosomes) of D_h ~ 250–500 nm (red symbols). Aqueous phase: Milli-Q water.

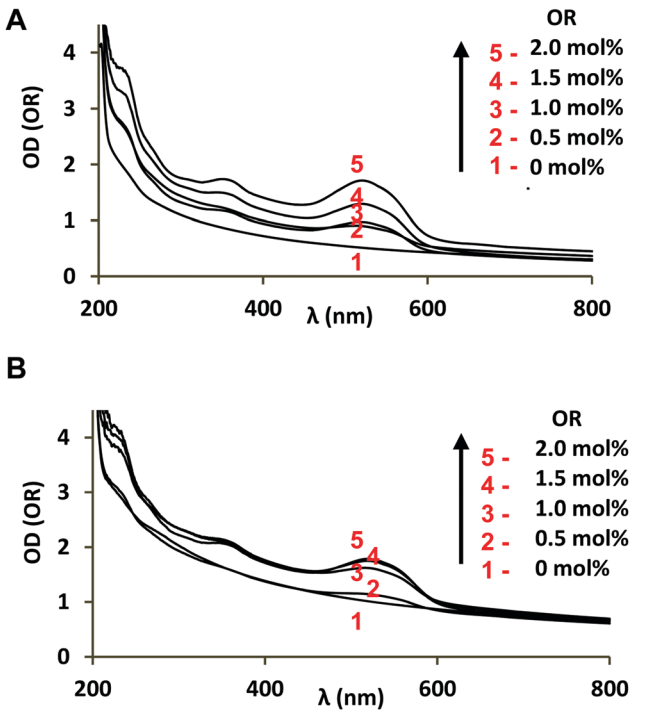

Fig. 7 Optical density (OD) plots derived from recording of UV-Vis spectra of Oil red (OR) solubilized in aqueous dispersions of MO/P80 and MO/P80/βCD-nC_{10} nanocarriers. The dispersed systems are prepared from mixed films containing 0.5, 1.0, 1.5 and 2 mol% OR with respect to the nonlamellar lipid MO. Temperature is 25 °C. Aqueous phase: Milli-Q water.

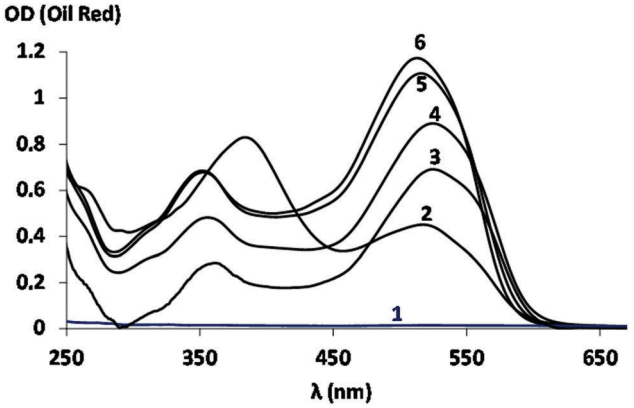

Fig. 8 Comparison of the UV-Vis spectra of Oil red (OR) solubilized in organic solvents of variable polarities (1: water, 2: chloroform; 4: ethylene glycol, 5: ethanol, 6: acetonitrile) with that of OR in amphiphilic nano-assemblies constituted of monoolein (MO), polysorbate 80 (P80) and β-CD-nC$_{10}$ (3: MO/P80/β-CD-nC$_{10}$) after subtraction of the nano-objects scattering. The concentration of Oil red in the organic solutions is 0.04 mM. Temperature is 25 °C.

optical density (OD) measurements and UV-Visible spectroscopy (Fig. 7). The lipophilic Oil red compound was completely insoluble in the aqueous phase as confirmed by the OD measurements. Its UV-Vis spectra were recorded upon solubilization in nanoassemblies with polysorbate P80 and in different organic solvents (Fig. 8). They revealed two major absorption bands with wavelength maxima (λ_{max}) at 359 and 516 nm and a notable absorbance at 280 nm. The dye was characterized by high molar extinction coefficients in organic solvent. A molar extinction coefficient ε_{OR} = 26994 L mol^{-1} cm^{-1} was determined for OR in ethanol solution at λ_{max} = 516 nm (ESI† Fig. S9).

The OD plots and UV-Vis spectra of OR in MO/P80 and MO/P80/β-CD-nC$_{10}$ nano-objects presented in Fig. 7, together with the results in ESI† Fig. S9–S11, were used for the quantification of the encapsulation efficiency in the cubosome nanocarriers with the help of an established protocol.[42] OR-loaded nanoparticles were dissolved in organic ethanol medium and the solution concentration was quantified using a standard curve. Towards treatment of the OD data of the MO/P80 and MO/P80/β-CD-nC$_{10}$ dispersions, the scattering background of the nano-objects was subtracted from the OD values through fitting by a power function in the wavelength region where OR does not have an absorption band (600–800 nm). Thus, the OR loading was evaluated from the fitted curves derived from Fig. 7 at the wavelength of maximal absorption and minimal turbidity. The scattering of the nano-objects was excluded from the optical signal. The wavelength of maximum absorption of OR formulated in nanoparticle dispersions was determined to be λ_{max} = 524 nm, whereas its λ_{max} was 516 nm in the organic solution (ethanol). This result, demonstrating the environmental sensitivity of the OR spectral response, suggested that the hydrophobic dye was solubilized in the lipid membranes of the studied self-assembled nanocarriers. The molar extinction coefficients of nanoencapsulated OR were estimated from the OD values determined at λ_{max} = 524 nm in the presence and absence of deep cavitands β-CD-nC$_{10}$ for the four different amounts of entrapped OR. The similarity of the values ε_1 = 18 450 ± 100 L mol^{-1} cm^{-1} (OR/MO/P80 nanodrug formulation) and ε_2 = 17 680 ± 100 L mol^{-1} cm^{-1} (OR/MO/P80/β-CD-nC$_{10}$ nanodrug formulation) indicated the preservation of the nanostructured environment of the OR chromophore in the two kinds of nanocarrier systems. Nevertheless, one can notice a slight difference provoked by the presence of β-CD-nC$_{10}$, which suggests that the local environment of the guest probe is modulated by the molecular composition of the host assemblies. The presence of the amphiphilic cyclodextrin (4 mol%) in the nanoassemblies did not dramatically influence the local environment polarity of OR in the mixed membranes. At variance, the quantitative estimations (based on Fig. 7 and ESI† Fig. S10, S11) revealed that βCD-nC$_{10}$ increases the affinity of OR for the lipid environment. For example, analytical determinations performed at 1.5 mol% OR in the mixed films allowed estimating that 80% of the initially introduced OR in the mixed membrane films is stably incorporated in the nanodrug-loaded carriers after sonication of the MO/P80 dispersions. Interestingly, this percentage increases to 91% for the MO/P80/β-CD-nC$_{10}$ assemblies. This may indicate that the obtained self-assembled nanocarriers are highly efficient for hydrophobic nanodrug encapsulation and transport.

Conclusion

In therapeutic innovation, the encapsulation efficiency is a major challenge and requires the design of novel drug delivery systems. Different kinds of supramolecular assemblies (liposomes, micelles, polymeric nanoparticles, *etc.*) have frequently been compared as carriers for solubilization of insoluble compounds of therapeutic interest. Cyclodextrin nanosponges and supramolecular scaffolds have attracted considerable interest recently in drug delivery applications.

In our work, βCD-nC$_{10}$ deep cavitand building blocks were used to generate liquid crystalline multicompartment nanocarriers comprising dual porosity. A typical feature of the proposed monoolein/βCD-nC$_{10}$ nanoparticle assemblies is the dynamic nature of the dispersed system forming cubosome structures at ambient temperature. After sonication, the 3D cubosomal assemblies coexist in the dispersion with a population of vesicular bilayer membranes. The deep cavitand βCD-nC$_{10}$ inserts in the lipid bilayers and stabilizes the cubosomal nanoparticle population. The quantity of βCD-nC$_{10}$ embedded in the membranes controls the formation of multicompartment nanocarriers through a shift of the vesicle-to-cubosome phase transition in favour of the cubic lattice nanoassemblies.

The cryo-TEM images and SAXS analyses established that the βCD-nC$_{10}$ deep cavitands induce crystalline order in the MO/P80 membrane assemblies. Both cryo-TEM and SAXS structural data revealed the formation of mixed lipid/βCD-nC$_{10}$ assemblies in which the deep cavitand favours the induction of primitive *Im*3*m* cubic lattice packing. The established cubic membrane structural organization of the nanocarriers suggests that they might be excellent candidates for sustained release of encapsulated fragile molecules. Quantitative determinations of

the nanoencapsulation of a model hydrophobic compound (Oil red) demonstrated that the encapsulation efficiency for the nanodrug may be as high as 91%. Further work will be required to establish the actual role of the amphiphilic deep cavitand βCD-nC_{10} in improving the capacity of the lipid nanocarriers to solubilize hydrophobic small molecular weight molecules.

Experimental section

Materials and sample preparation

Polysorbate 80 (P80) (MW 1310, CMC 0.012 mM) and monoolein (MO) (≥99%, MW 356.54) were products obtained from Sigma-Aldrich (St. Quentin Falavier). The amphiphilic cyclodextrin β-CD-nC_{10} with a degree of substitution by decanoate (C_{10}) chains of n = 7.3 (determined by MALDI-TOF analysis) had an average molecular weight MW of 2266 (batch LCH3-36). The compound was produced through enzymatic transesterification of β-CD with vinyl decanoate using thermolysin as a catalyzer as previously reported.[25b] The model hydrophobic compound 1-[2,5-dimethyl-4-(2,5-dimethylphenylazo)phenylazo]-2-naphthol certified as a fat stain for microscopy of biological samples under the name Oil red O (OR) (MW 408.49) was purchased from Sigma-Aldrich (St. Quentin Falavier). Milli-Q water of resistivity 18.2 MΩ cm (Millipore Co.) was used as the aqueous phase.

The organic thin film hydration method[5b,6d] was used to prepare MO/P80, MO/P80/OR, MO/P80/βCD-nC_{10} and MO/P80/βCD-nC_{10}/OR nanoparticles. In a preliminary study, the content of the amphiphilic deep cavitand was varied from 1 to 10 mol% βCD-nC_{10} and subsequently fixed to 4 mol% in this work. The amphiphilic components and the Oil red dye were dissolved in chloroform. Liquid mixtures were obtained by precise aliquoting of calculated volumes of stock solutions of every constituent. After mixing, the organic solvent was evaporated under the flow of nitrogen gas and the obtained multicomponent organic thin films were lyophilized overnight. The hydration of the films was performed in excess of the Milli-Q water phase. For preparation of nanoparticle dispersions (2 mL samples), the lipid concentration was around 10 mg mL^{-1}. The mixed films contained in this case the surfactant P80 exerting the role of a dispersing agent of the bulk liquid crystalline phase. Multiple cycles of vortexing and ice bath sonication (Branson 2510) were applied to ensure the homogeneity of the dispersed assemblies. The samples were kept at room temperature and investigated at 25 °C after 10× dilution prior to optical measurements. For bulk mesophase studies by POM, the thin film hydration was done at the 50 wt% lipid phase in Milli-Q water (50/50 w/w).

Methods

Cryogenic transmission electron microscopy (cryo-TEM) setup. For cryo-TEM imaging, a drop of nano-object suspension (5–10 mg mL^{-1}) was deposited on a freshly glow-discharged (easiGlow, Pelco) lacy carbon film (NetMesh, Pelco) supported by a copper grid. The grid, held by tweezers, was placed in the chamber of the fast-freezing Leica EM-GP workstation, where the relative humidity was kept at 85%. The excess liquid was absorbed using filter paper and the grid was immediately plunged into liquid ethane (−185 °C). It was then mounted on a Gatan 626 specimen holder precooled with liquid nitrogen, and transferred to the microscope. The samples were observed at −176 °C, under low electron beam illumination, using a Philips CM200 'Cryo' transmission electron microscope operating at 80 kV. The images were recorded on Kodak SO163 films using the ''Low Dose'' Philips procedure, which limits the radiation damage in the region of interest prior to actual image recording. The negatives were subsequently scanned by a planar scanner and analyzed using *Image J* software.

Small-angle X-ray scattering (SAXS) setup. Small-angle X-ray scattering experiments were performed at the bending magnet beamline B21 at the Diamond Light Source synchrotron (Didcot, UK). The X-ray wavelength and the sample-to-detector distance were 0.1 nm and 3.9 m, respectively, corresponding to an accessible q-range of 0.07 to 3.2 nm^{-1}. The 2D SAXS patterns were recorded using a high-sensitivity zero noise Pilatus 2M detector having an active area of 254 mm × 289 mm, which was divided into 1679 × 1475 pixels. The data acquisition sequence was hardware triggered by a robotized injection device. Each SAXS pattern was measured over 1 s. The incident and transmitted beam intensities were recorded simultaneously with every SAXS frame. After each data acquisition sequence, the obtained 2D images were corrected for the detector spatial response function, and normalized by transmission. Normalized 2D patterns were subsequently azimuthally averaged to obtain the 1D scattering curves. Multiple patterns of the scattering background from the quartz sample holder (1.6 mm capillary *in vacuo*) and the solvent were measured and processed in the same way, averaged, and subtracted from the acquired data using the SAXS BL21 software. The model[41] of Garstecki and Holyst was employed in the SAXS data fitting and determination of the structural parameters of the lipid cubic structures.

Polarized optical microscopy (POM). The experimental setup included a microscope Nikon Eclipse E600 equipped with a polarizer and a Mightex Buffer USB camera (Mightex Systems). Objectives with magnifications of ×20 and ×10 were employed. Liquid crystalline samples were studied in the form of hydrated thin organic films situated between two cover glass slides. The cell, protecting the samples from dehydration, was inserted in a temperature-controlled stage and examined under cross polarizers by POM.

Particle size measurements by quasi-elastic light scattering (QELS). Hydrodynamic particle diameters were determined by quasi-elastic light scattering. The measurements were performed using a Zetasizer Nano ZS-90 instrument (Malvern) equipped with a He–Ne laser (633 nm) with a power 5 mW. A fixed scattering angle of 90° was employed. The measurements were performed in triplicate for every sample after a 10× dilution in MilliQ water of the stock nanoparticle dispersion (2 mL). The temperature was 25 °C. The mean hydrodynamic diameters were determined under approximation of the dispersed objects by equivalent spherical shapes. The nanoparticle populations were analyzed in the multimodal mode provided by the software of

the Malvern apparatus. Reproducible results were obtained with all kinds of investigated amphiphilic mixtures.

UV-Visible spectroscopy and optical density measurements. Optical density (OD) and UV-Visible spectroscopy measurements were performed using a Perkin-Elmer Lambda 35 double beam UV-Visible spectrophotometer (Perkin Elmer, France). The UV-Visible spectra of the dye Oil red (OR) were studied in organic solvents, micellar solutions of P80, and in aqueous dispersions of self-assembled nanocarriers. For optical density measurements, the dispersions encapsulating OR were diluted 10 times in MilliQ water. The studied wavelength region was 200–800 nm. Optical density curves were acquired in the presence and absence of OR dye in the systems. Nano-assemblies MO/P80/OR/βCD-C_{10} of variable encapsulated quantities of OR were examined at constant lipid and amphiphile contents. The nanoparticle sizes were determined in parallel by QELS. The MO/P80/OR/βCD-C_{10} dispersed systems of various compositions were placed in 1 cm optical quartz cuvettes thermostated at 25 °C. The molar extinction coefficients of OR were determined either in ethanol solvent at a wavelength of 516 nm or in nanoparticulate systems at a wavelength of 524 nm. The encapsulation efficiency of OR was determined using an established protocol[42] based on spectral data recorded at different OR contents.

Acknowledgements

The financial support from ANR SIMI10 Nanosciences to the project CYDEXCAR (ANR-11-BS10-0007) is gratefully acknowledged. L. Z. received a PhD scholarship from Agence Nationale de la Recherche. B. A. is supported by the project ELI – Extreme Light Infrastructure – phase 2 (CZ.02.1.01/0.0/0.0/15_008/0000162) from European Regional Development Fund. J.-J. Vachon is acknowledged for assistance with the polarized optical microscopy setup. The authors thank the Diamond Light Source (Didcot, UK) for granting SAXS beam time at the B21 beamline, as well as the Electron Microscopy facility of the NanoBio-ICMG Chemistry Platform (Grenoble) for granting access to the cryo-TEM equipment.

References

1 (*a*) A. Yaghmur and O. Glatter, *Adv. Colloid Interface Sci.*, 2009, **147–148**, 333; (*b*) C. V. Kulkarni, R. Mezzenga and O. Glatter, *Soft Matter*, 2010, **6**, 5615.

2 (*a*) A. Zabara, R. Negrini, P. Baumann, O. Onaca-Fischer and R. Mezzenga, *Chem. Commun.*, 2014, **50**, 2642; (*b*) C. E. Conn and C. J. Drummond, *Soft Matter*, 2013, **9**, 3449.

3 (*a*) A. Zabara and R. Mezzenga, *J. Controlled Release*, 2014, **188**, 31; (*b*) A. Angelova, B. Angelov, R. Mutafchieva and S. Lesieur, *J. Inorg. Organomet. Polym. Mater.*, 2015, **25**, 214; (*c*) I. D. M. Azmi, L. P. Wu, P. P. Wibroe, C. Nilsson, J. Ostergaard, S. Sturup, B. Gammelgaard, A. Urtti, S. M. Moghimi and A. Yaghmur, *Langmuir*, 2015, **31**, 5042; (*d*) A. Angelova, B. Angelov, R. Mutafchieva, S. Lesieur and P. Couvreur, *Acc. Chem. Res.*, 2011, **44**, 147.

4 (*a*) A. Sadeghpour, F. Pirolt, G. R. Iglesias and O. Glatter, *Langmuir*, 2014, **30**, 2639; (*b*) W. J. Sun, J. J. Vallooran and R. Mezzenga, *Langmuir*, 2015, **31**, 4558; (*c*) C. V. Kulkarni, T. Y. Tang, A. M. Seddon, J. M. Seddon, O. Ces and R. H. Templer, *Soft Matter*, 2010, **6**, 3191; (*d*) B. Angelov, A. Angelova, S. K. Filippov, M. Drechsler, P. Štěpánek and S. Lesieur, *ACS Nano*, 2014, **8**, 5216.

5 (*a*) R. Negrini and R. Mezzenga, *Langmuir*, 2011, **27**, 5296; (*b*) B. Angelov, A. Angelova, S. K. Filippov, G. Karlsson, N. Terrill, S. Lesieur and P. Štěpánek, *Soft Matter*, 2011, **7**, 9714; (*c*) W. K. Fong, S. Salentinig, C. A. Prestidge, R. Mezzenga, A. Hawley and B. J. Boyd, *Langmuir*, 2014, **30**, 5373; (*d*) B. Angelov, A. Angelova, S. K. Filippov, T. Narayanan, M. Drechsler, P. Štěpánek, P. Couvreur and S. Lesieur, *J. Phys. Chem. Lett.*, 2013, **4**, 1959.

6 (*a*) C. Nilsson, J. Østergaard, S. W. Larsen, C. Larsen, A. Urtti and A. Yaghmur, *Langmuir*, 2014, **30**, 6398; (*b*) A. Angelova, B. Angelov, B. Papahadjopoulos-Sternberg, C. Bourgaux and P. Couvreur, *J. Phys. Chem. B*, 2005, **109**, 3089; (*c*) S. F. Hedegaard, C. Nilsson, P. Laurinmaki, S. Butcher, A. Urtti and A. Yaghmur, *RSC Adv.*, 2013, **3**, 24576; (*d*) A. Angelova, B. Angelov, M. Drechsler, V. M. Garamus and S. Lesieur, *Int. J. Pharm.*, 2013, **454**, 625.

7 (*a*) C. V. Kulkarni, Z. Moinuddin, R. Littlefield, Y. Patil-Sen and M. Hood, *Int. J. Pharm.*, 2015, **479**, 416; (*b*) M. Wadsater, J. Barauskas, T. Nylander and F. Tiberg, *ACS Appl. Mater. Interfaces*, 2014, **6**, 7063; (*c*) A. Angelova, B. Angelov, M. Drechsler and S. Lesieur, *Drug Discovery Today*, 2013, **18**, 1263.

8 (*a*) C. V. Kulkarni, O. Ces, R. H. Templer and J. M. Seddon, *Soft Matter*, 2013, **9**, 6525; (*b*) A. Angelova, B. Angelov, B. Papahadjopoulos-Sternberg, M. Ollivon and C. Bourgaux, *J. Drug Delivery Sci. Technol.*, 2005, **15**, 108; (*c*) B. Angelov, A. Angelova, V. M. Garamus, M. Drechsler, R. Willumeit, R. Mutafchieva, P. Štěpánek and S. Lesieur, *Langmuir*, 2012, **28**, 16647; (*d*) H. H. Shen, V. Lake, A. P. Le Brun, M. James, A. P. Duff, Y. Peng, K. M. McLean and P. G. Hartley, *Biomaterials*, 2013, **34**, 8361.

9 (*a*) H. M. G. Barriga, A. I. I. Tyler, N. L. C. McCarthy, E. S. Parsons, O. Ces, R. V. Law, J. M. Seddon and N. J. Brooks, *Soft Matter*, 2015, **11**, 600; (*b*) W. K. Fong, T. Hanley, B. Thierry, N. Kirby and B. J. Boyd, *Langmuir*, 2010, **26**, 6136; (*c*) A. Angelova, B. Angelov, V. M. Garamus, P. Couvreur and S. Lesieur, *J. Phys. Chem. Lett.*, 2012, **3**, 445; (*d*) N. K. Swarnakar, K. Thanki and S. Jain, *Mol. Pharmaceutics*, 2014, **11**, 1435.

10 (*a*) P. T. Spicer, *Curr. Opin. Colloid Interface Sci.*, 2005, **10**, 274; (*b*) P. T. Spicer, W. B. Small, M. L. Lynch and J. L. Burns, *J. Nanopart. Res.*, 2002, **4**, 297; (*c*) B. Angelov, A. Angelova, B. Papahadjopoulos-Sternberg, S. Lesieur, J.-F. Sadoc, M. Ollivon and P. Couvreur, *J. Am. Chem. Soc.*, 2006, **128**, 5813; (*d*) D. Yang, B. Armitage and S. R. Marder, *Angew. Chem., Int. Ed.*, 2004, **43**, 4402.

11 (*a*) E. Esposito, P. Mariani, L. Ravani, C. Contado, M. Volta, S. Bido, M. Drechsler, S. Mazzoni, E. Menegatti, M. Morari

and R. Cortesi, *Eur. J. Pharm. Biopharm.*, 2012, **80**, 306; (*b*) B. Angelov, A. Angelova, M. Ollivon, C. Bourgaux and J. Campitelli, *J. Am. Chem. Soc.*, 2003, **125**, 7188; (*c*) G. Mangiapia, M. Vaccaro, G. D'Errico, H. Frielinghaus, A. Radulescu, V. Pipich, A. M. Carnerup and L. Paduano, *Soft Matter*, 2011, **7**, 10577; (*d*) M. Komisarski, Y. M. Osornio, J. S. Siegel and E. M. Landau, *Chem. – Eur. J.*, 2013, **19**, 1262.

12 (*a*) A. W. Dong, C. Fong, L. J. Waddington, A. J. Hill, B. Boyd and C. J. Drummond, *Phys. Chem. Chem. Phys.*, 2015, **17**, 1705; (*b*) B. Angelov, A. Angelova, M. Drechsler, V. M. Garamus, R. Mutafchieva and S. Lesieur, *Soft Matter*, 2015, **11**, 3686; (*c*) E. Nazaruk, M. Szlezak, E. Gorecka, R. Bilewicz, Y. M. Osornio, P. Uebelhart and E. M. Landau, *Langmuir*, 2014, **30**, 1383; (*d*) J. Barauskas, L. Christerson, M. Wadsäter, F. Lindström, A. K. Lindqvist and F. Tiberg, *Mol. Pharmaceutics*, 2014, **11**, 895.

13 (*a*) N. Rahanyan-Kaegi, S. Aleandri, C. Speziale, R. Mezzenga and E. M. Landau, *Chem. – Eur. J.*, 2015, **21**, 1873; (*b*) A. Angelova, B. Angelov, S. Lesieur, R. Mutafchieva, M. Ollivon, C. Bourgaux, R. Willumeit and P. Couvreur, *J. Drug Delivery Sci. Technol.*, 2008, **18**, 41; (*c*) S. B. Rizwan, W. T. McBurney, K. Young, T. Hanley, B. J. Boyd, T. Rades and S. Hook, *J. Controlled Release*, 2013, **165**, 16; (*d*) T. E. Hartnett, K. Ladewig, A. J. O'Connor, P. G. Hartley and K. M. McLean, *RSC Adv.*, 2015, **3**, 26543.

14 (*a*) Y.-D. Dong, A. J. Tilley, I. Larson, M. J. Lawrence, H. Amenitsch, M. Rappolt, T. Hanley and B. J. Boyd, *Langmuir*, 2010, **26**, 9000; (*b*) B. Angelov, A. Angelova, U. Vainio, V. M. Garamus, S. Lesieur, R. Willumeit and P. Couvreur, *Langmuir*, 2009, **25**, 3734; (*c*) E. Esposito, L. Ravani, C. Contado, A. Costenaro, M. Drechsler, D. Rossi, E. Menegatti, A. Grandini and R. Cortesi, *Mater. Sci. Eng., C*, 2013, **33**, 411.

15 (*a*) A. Yaghmur, B. Sartori and M. Rappolt, *Phys. Chem. Chem. Phys.*, 2011, **13**, 3115; (*b*) T. H. Nguyen, T. Hanley, C. J. Poter and B. J. Boyd, *J. Controlled Release*, 2011, **153**, 180; (*c*) N. Tran, X. Mulet, A. M. Hawley, C. E. Conn, J. Zhai, L. J. Waddington and C. J. Drummond, *Nano Lett.*, 2015, **15**, 4229.

16 (*a*) J. Kubitschke, S. Javor and J. Rebek Jr., *Chem. Commun.*, 2012, **48**, 9251–9253; (*b*) Y. Chen, A. Angelova, B. Angelov, M. Drechsler, V. M. Garamus, R. Willumeit-Römer and A. Zou, *J. Mater. Chem. B*, 2015, **3**, 7734.

17 (*a*) A. Singireddy and S. Subramanian, *J. Mater. Sci.*, 2014, **49**, 8140; (*b*) R. Minelli, R. Cavalli, L. Ellis, P. Pettazzoni, F. Trotta, E. Ciamporcero, G. Barrera, R. Fantozzi, C. Dianzani and R. Pili, *Eur. J. Pharm. Sci.*, 2012, **47**, 686; (*c*) S. S. Darandale and R. P. Vavia, *J. Inclusion Phenom. Macrocyclic Chem.*, 2013, **75**, 315.

18 (*a*) J. B. G. Yaméogo, A. Gèze, L. Choisnard, J.-L. Putaux, A. Gansané, S. B. Sirima, R. Semdé and D. Wouessidjewe, *Eur. J. Pharm. Biopharm.*, 2012, **80**, 508; (*b*) S. M. N. Simoes, A. Rey-Rico, A. Concheiro and C. Alvarez-Lorenzo, *Chem. Commun.*, 2015, **51**, 6275; (*c*) M. D. Moya-Ortega, C. Alvarez-Lorenzo, A. Concheiro and T. Loftsson, *Int. J. Pharm.*, 2012, **428**, 152; (*d*) E. Bilensoy, O. Gürkaynak, M. Ertan, M. Sen and A. A. Hincal, *J. Pharm. Sci.*, 2008, **97**, 1519.

19 (*a*) F. J. Otero-Espinar, J. J. Torres-Labandeira, C. Alvarez-Lorenzo and J. Blanco-Méndez, *J. Drug Delivery Sci. Technol.*, 2010, **20**, 289; (*b*) W. F. Lai, *Biomaterials*, 2014, **35**, 401; (*c*) C. Machut-Binkowski, F. Hapiot, R. Cecchelli, P. Martin and E. A. Monflier, *J. Inclusion Phenom. Macrocyclic Chem.*, 2007, **57**, 567.

20 (*a*) E. Bilensoy, O. Gürkaynak, A. L. Doğan and A. A. Hıncal, *Int. J. Pharm.*, 2008, **347**, 163; (*b*) M. Massaro, S. Piana, C. G. Colletti, R. Noto, S. Riela, C. Baiamonte, C. Giordano, G. Pizzolanti, G. Cavallaro, S. Milioto and G. Lazzara, *J. Mater. Chem. B*, 2015, **3**, 4074; (*c*) F. Quaglia, L. Ostacolo, A. Mazzaglia, V. Villari, D. Zaccaria and M. T. Sciortino, *Biomaterials*, 2009, **30**, 374; (*d*) J. Zhang and P. X. Ma, *Adv. Drug Delivery Rev.*, 2013, **65**, 1215.

21 (*a*) B. M. D. C. Godinho, J. R. Ogier, A. Quinlan, R. Darcy, B. T. Griffin, J. F. Cryan and C. M. Driscoll, *Int. J. Pharm.*, 2014, **473**, 105; (*b*) R. Rajendiran, R. K. Sankaranarayanan and J. Saravanan, *J. Mol. Struct.*, 2014, **1067**, 252; (*c*) E. Pinho, M. Grootveld, S. Soares Graça and M. Henriques, *Carbohydr. Polym.*, 2014, **101**, 121.

22 (*a*) M. Vecsernyés, F. Fenyvesi, I. Bacskay, M. A. Deli, L. Szente and E. Fenyvesi, *Arch. Med. Res.*, 2014, 1; (*b*) F. Perret, M. Duffour, Y. Chevalier and H. Parrot-Lopez, *Eur. J. Pharm. Biopharm.*, 2013, **83**, 25; (*c*) J. M. Lopez-Nicolas, P. Rodriguez-Bonilla and F. Garcia-Carmona, *Crit. Rev. Food Sci. Nutr.*, 2014, **54**, 251.

23 (*a*) R. Challa, A. Ahuja, J. Ali and R. K. Khar, *Pharm. Sci. Technol.*, 2005, **6**, 329; (*b*) S. Y. Zhou, S. X. Ma, H. L. Cheng, L. J. Yang, W. Chen, Y. Q. Yin, Y. M. Shi and X. D. Yang, *J. Mol. Struct.*, 2014, **1058**, 181; (*c*) S. M. Seyedi, H. Sadeghian, A. Jabbari, A. Assadi and H. Momeni, *Tetrahedron*, 2010, **66**, 6754; (*d*) S. M. Seyedi, H. Sadeghian, A. Jabbari, A. Assadieskandar and H. Momeni, *Bioorg. Med. Chem.*, 2011, **19**, 4307.

24 (*a*) F. Perret, C. Marminon, W. Zeinyeh, P. Nebois, A. Bollacke, J. Jose, H. Parrot-Lopez and M. Le Borgne, *Int. J. Pharm.*, 2013, **441**, 491; (*b*) A. Mazzaglia, M. L. Bondì, A. Scala, F. Zito, G. Barbieri, F. Crea, G. Vianelli, P. Mineo, T. Fiore, G. Pellerito, L. Pellerito and M. A. Costa, *Biomacromolecules*, 2013, **14**, 3820; (*c*) A. M. O'Mahony, D. Doyle, R. Darcy, J.-F. Cryan and C. M. O'Driscoll, *Eur. J. Pharm. Sci.*, 2012, **47**, 896.

25 (*a*) J. B. G. Yaméogo, A. Gèze, L. Choisnard, J.-L. Putaux, R. Semdé and D. Wouessidjewe, *Curr. Top. Med. Chem.*, 2014, **14**, 526; (*b*) L. Choisnard, A. Gèze, C. Vanhaverbeke, J. B. G. Yaméogo, J.-L. Putaux, B. Brasme, L. Jullien, S. Boullanger, C. Elfakir and D. Wouessidjewe, *Biomacromolecules*, 2011, **12**, 3031; (*c*) L. Choisnard, A. Gèze, J.-L. Putaux, Y.-S. Wong and D. Wouessidjewe, *Biomacromolecules*, 2006, **7**, 515; (*d*) M. Roux, B. Perly and F. Djedaïni-Pilard, *Eur. Biophys. J.*, 2007, **36**, 861.

26 (*a*) L. Choisnard, A. Gèze, B. G. J. Yaméogo, J.-L. Putaux and D. Wouessidjewe, *Int. J. Pharm.*, 2007, **344**, 26; (*b*) A. Angelova, C. Fajolles, C. Hocquelet, F. Djedaïni-Pilard, S. Lesieur,

V. Bonnet, B. Perly, G. Le Bas and L. Mauclaire, *J. Colloid Interface Sci.*, 2008, **322**, 304; (*c*) R. Cavalli, F. Trotta, M. E. Carlotti, B. Possetti and M. Trotta, *J. Inclusion Phenom. Macrocyclic Chem.*, 2007, **57**, 657; (*d*) J. Li and X. J. Loh, *Adv. Drug Delivery Rev.*, 2008, **60**, 1000.

27 (*a*) R. Villalonga, R. Cao and A. Fragoso, *Chem. Rev.*, 2007, **107**, 3088; (*b*) G. Crini, *Chem. Rev.*, 2014, **114**, 10940; (*c*) L. Zerkoune, A. Angelova, L. Choisnard, A. Gèze, D. Wouessidjewe and S. Lesieur, *ICOMF14 Proceedings*, MATEC Web of Conferences, EDP Sciences publisher, 2013, **4**, 05001; (*d*) T. Aree, *J. Inclusion Phenom. Macrocyclic Chem.*, 2013, **77**, 439.

28 (*a*) F. L. Callari, A. Mazzaglia, L. Monsù Scolaro, L. Valli and S. Sortino, *J. Mater. Chem.*, 2008, **18**, 802; (*b*) A. Angelova, C. Ringard-Lefebvre and A. Baszkin, *J. Colloid Interface Sci.*, 1999, **212**, 275; (*c*) A. Angelova, C. Ringard-Lefebvre and A. Baszkin, *J. Colloid Interface Sci.*, 1999, **212**, 280.

29 (*a*) L. Zerkoune, A. Angelova and S. Lesieur, *Nanomaterials*, 2014, **4**, 741; (*b*) H. Parrot-Lopez, F. Perret and B. Bertino-Ghera, *Ann. Pharm. Fr.*, 2010, **68**, 12; (*c*) N. Zafar, H. Fessi and A. Elaissari, *Int. J. Pharm.*, 2014, **461**, 351.

30 (*a*) D. Gallois-Montbrun, G. Le Bas, S. Mason, A. Sax, T. Prange and S. Lesieur, *Acta Crystallogr., Sect. B: Struct. Sci., Cryst. Eng. Mater.*, 2013, **69**, 214; (*b*) V. Bernat, C. Ringard-Lefebvre, G. Le Bas, B. Perly, F. Djedaini-Pilard and S. Lesieur, *Langmuir*, 2008, **24**, 3140; (*c*) T. Sun, H. Zhang, L. Kong, H. Qiao, Y. Li, F. Xin and A. Hao, *Carbohydr. Res.*, 2011, **346**, 285.

31 (*a*) A. Gèze, S. Aous, I. Baussanne, J.-L. Putaux, J. Defaye and D. Wouessidjewe, *Int. J. Pharm.*, 2002, **242**, 301; (*b*) A. Gèze, L. Choisnard, J. L. Putaux and D. Wouessidjewe, *Mater. Sci. Eng., C*, 2009, **29**, 458.

32 (*a*) M. Messner, S. V. Kurkov, P. Jansook and T. Loftsson, *Int. J. Pharm.*, 2010, **387**, 199–208; (*b*) G. Chen and M. Jiang, *Chem. Soc. Rev.*, 2011, **40**, 2254; (*c*) Q.-D. Hu, G.-P. Tang and P. K. Chu, *Acc. Chem. Res.*, 2014, **7**, 2017; (*d*) Y. Chen and Y. Liu, *Chem. Soc. Rev.*, 2010, **39**, 495.

33 (*a*) M. Ramanathan, L. K. Shrestha, T. Mori, Q. Ji, J. P. Hill and K. Ariga, *Phys. Chem. Chem. Phys.*, 2013, **15**, 10580; (*b*) A. Angelova, F. Penacorada, B. Stiller, T. Zetzsche, R. Ionov, H. Kamusewitz and L. Brehmer, *J. Phys. Chem.*, 1994, **98**, 6790; (*c*) J. G. Petrov and A. Angelova, *Langmuir*, 1992, **8**, 3109; (*d*) A. Angelova, J. Reiche, R. Ionov, D. Janietz and L. Brehmer, *Thin Solid Films*, 1994, **242**, 289.

34 (*a*) M. Cano-Sarabia, A. Angelova, N. Ventosa, S. Lesieur and J. Vecina, *J. Colloid Interface Sci.*, 2010, **350**, 10; (*b*) J. G. Petrov, D. Mobius and A. Angelova, *Langmuir*, 1992, **8**, 201; (*c*) J. G. Petrov, A. Angelova and D. Mobius, *Langmuir*, 1992, **8**, 206.

35 (*a*) D. Bennet, M. Marimuthu, S. Kim and J. An, *Int. J. Nanomed.*, 2012, **7**, 3399; (*b*) Y. Mi, J. Zhao and S. S. Feng, *J. Controlled Release*, 2013, **169**, 185; (*c*) F. Zhao, H. Yin and J. Li, *Biomaterials*, 2014, **35**, 1050; (*d*) T. Liu, W. Xue, B. Ke, M. Q. Xie and M. Dong, *Biomaterials*, 2014, **35**, 3865.

36 (*a*) C. Kim, B. P. Shah, P. Subramaniam and K. B. Lee, *Mol. Pharmaceutics*, 2011, **8**, 1955; (*b*) S. Sreenivasan and S. Krishnakumar, *Curr. Eye Res.*, 2014, **12**, 1; (*c*) Y. D. Wen, Y. L. Ho, R. J. Shiau, J. K. Yeh, J. Y. Wu, W. L. Wang and S. J. Chiou, *J. Organomet. Chem.*, 2010, **695**, 352; (*d*) T. Liu, M. Wang, T. Wang, Y. Yao and N. Zhang, *Colloids Surf., B*, 2015, **126**, 531.

37 (*a*) E. Markovsky, H. Baabur-Cohen and R. Satchi-Fainaro, *J. Controlled Release*, 2014, **187**, 145; (*b*) V. Jain, N. K. Swarnakar, P. R. Mishra, A. Verma, A. K. Mishra and N. K. Jain, *Biomaterials*, 2012, **33**, 7206; (*c*) H. Richly, B. Schultheis, I. A. Adamietz, P. Kupsch, M. Grubert, R. A. Hilger, M. Ludwig, E. Brendel, O. Christensen and D. Strumberg, *Eur. J. Cancer*, 2009, **45**, 579.

38 (*a*) N. Kolishetti, S. Dhar, P. M. Valencia, L. Q. Lin, R. Karnik, S. J. Lippard, R. Langer and O. C. Farokhzad, *Proc. Natl. Acad. Sci. U. S. A.*, 2010, **107**, 17939; (*b*) C. Kim, B. P. Shah, P. Subramaniam and K. B. Lee, *Mol. Pharmaceutics*, 2011, **8**, 1955; (*c*) F. Zhao, H. Yin and J. Li, *Biomaterials*, 2014, **35**, 1050.

39 (*a*) C. V. Kulkarni, W. Wachter, G. Iglesias-Salto, S. Engelskirchen and S. Ahualli, *Phys. Chem. Chem. Phys.*, 2011, **13**, 3004; (*b*) V. Cherezov, J. Clogston, M. Z. Papiz and M. Caffrey, *J. Mol. Biol.*, 2006, **357**, 1605; (*c*) L. V. Misquitta, Y. Misquitta, V. Cherezov, O. Slattery, J. M. Mohan, D. Hart, M. Zhalnina, W. A. Cramer and M. Caffrey, *Structure*, 2004, **12**, 2113.

40 H. Azhari, M. Strauss, S. Hook, B. Boyd and S. B. Rizwan, *Eur. J. Pharm. Biopharm.*, 2016, **104**, 148.

41 (*a*) P. Garstecki and R. Holyst, *Langmuir*, 2002, **18**, 2529; (*b*) P. Garstecki and R. Hoyst, *Langmuir*, 2002, **18**, 2519.

42 J. A. Ankrum, O. R. Miranda, K. S. Ng, D. Sarkar, C. Xu and J. M. Karp, *Nat. Protoc.*, 2014, **9**, 233.

